Acta Crystallographica Section D
Biological Crystallography
ISSN 0907-4449

Systematic analysis of supersaturation and lysozyme crystal quality

Izumi Yoshizaki,[a,b]* Takao Sato,[c] Noriyuki Igarashi,[d] Makoto Natsuisaka,[b] Nobuo Tanaka,[c] Hiroshi Komatsu[b,e] and Shinichi Yoda[a,b]

[a]Department of Innovative and Engineered Materials, Interdisciplinary Graduate School of Science and Engineering, Tokyo Institute of Technology, 4259 Nagatsuta, Midori-ku, Yokohama 226-8502, Japan, [b]National Space Development Agency of Japan (NASDA), Space Utilization Research Center, 2-1-1 Sengen, Tsukuba 305-8505, Japan, [c]Department of Life Science, Graduate School of Bioscience and Biotechnology, Tokyo Institute of Technology, 4259 Nagatsuta, Midori-ku, Yokohama 226-8501, Japan, [d]Institute of Materials Structure Science, High Energy Accelerator Research Organization, 1-1 Oho, Tsukuba 305-0801, Japan, and [e]Iwate Prefectural University, Takizawa-mura, Iwate 020-0193, Japan

Correspondence e-mail: yoshizaki.izumi@nasda.go.jp

Received 1 March 2001
Accepted 15 August 2001

A systematic study of the correlation between supersaturation and protein crystal quality was carried out employing atomic force microscopy (AFM) and X-ray crystallography with synchrotron radiation (SR). The surface morphology and growth rates of hen egg-white (HEW) lysozyme crystals soaked in various supersaturated solutions were first investigated by AFM. The results showed that the formation of two-dimensional islands increased as a function of supersaturation. The growth rate (molecule intake speed) also increased as a function of supersaturation. In order to examine the correlation between the surface morphology, growth rate and the crystal quality, X-ray diffraction experiments were performed. It was confirmed that crystals grown at lower supersaturations diffracted better with higher signal-to-noise ratios, including better agreement between symmetry-related reflections. The results strongly suggested that the molecular misorientation at high supersaturation affected the crystal quality.

1. Introduction

The importance of the three-dimensional structures of macromolecules has been widely recognized for many years. Structural molecular biology has become a powerful tool for understanding enzyme function and treatment of diseases. As structure-based drug design has proved its value, the demand for the determination of three-dimensional structures of proteins has increased. However, the bottleneck in three-dimensional structure determination still remains the growth of high-quality protein crystals. Many attempts have been made to produce better diffracting crystals by determining the optimum growth conditions (choosing the proper precipitant, buffer, concentration and temperature), using different crystallization methods and so on.

One of the most important experimental parameters in crystal growth is supersaturation, irrespective of the growth method. Supersaturation (S) is defined as $S = (C - \mathrm{Ce})/\mathrm{Ce}$, where C is the protein concentration and Ce is the protein solubility (with the same precipitant concentration, buffer and temperature). Changing the protein concentration or temperature changes the supersaturation. The driving force of crystal growth ($\Delta\mu$) is a function of supersaturation [$\Delta\mu = kT\ln(C/\mathrm{Ce}) = kT\ln(1 + S)$, where k is Boltzmann's constant and T is temperature]. Growth rates are direct functions of supersaturation (Chernov, 1984).

Empirically, it was well known that crystals that grew more slowly looked better and also diffracted better. Therefore, a low supersaturated solution was used in some studies to obtain better crystals by growing them slowly (Saridakis *et al.*, 1994).

However, no crystallographic study has yet explained the direct correlation of supersaturation and crystal quality, although less systematic research has been performed in terms of protein crystal growth.

If supersaturation affects the crystal quality, the next question is: why would high supersaturation affect the crystal quality?

Fast crystal growth can result in molecules being trapped in high-energy (non-stable) configurations at a kink site inconsistent with the regular periodic lattice (Boggon *et al.*, 2000). This is possible because the protein molecule is anisotropic both in shape and bonding site. Also, the amino-acid side chains of the protein molecules are not strictly rigid in structure, so they may arrange their residues to fit in the kink site even if they were misoriented. However, it is difficult to prove this hypothesis, since observing the orientation of each protein molecule is impossible at present.

Incorporation of defects may be enhanced at high supersaturation. From a macroscopic point of view, surface morphology studies as a function of supersaturation have been reported (Ng *et al.*, 1997). They observed the tRNA crystal surface at various temperatures. At higher temperature (low supersaturation), spiral growth was observed. At lower temperature (moderate supersaturation), two-dimansional (2D) nucleation growth was observed. At even lower temperature (high supersaturation), three-dimensional (3D) nucleation and mutilayer stack macrostep formation was observed. Preliminary X-ray diffraction experiments were also carried out and it was found that crystals that grew at high supersaturation diffracted to only 6 Å and that crystals that grew at lower supersaturation diffracted to 4 Å. However, this X-ray study was preliminary and no systematic analysis was presented. Crystal properties vary even under the same crystallization conditions (Judge *et al.*, 1999), so the correlation of supersaturation, growth condition and crystal quality should be discussed carefully.

Nucleation frequency is also a function of supersaturation, so as the supersaturation increases the more the nucleus forms in the bulk solution and may well be incorporated into the mother crystal. Uncontrolled nucleation can be avoided by growing the crystals at a very low supersaturation, as nucleation requires a higher driving force than crystal growth. This is called the metastable zone. Stura & Wilson (1992) introduced a seeding technique in order to avoid uncontrolled nucleation by growing the seeds in a metastable zone. Several experiments were performed to obtain better crystals by growing them in the metastable zone, but only crystal size data were reported (Saridakis *et al.*, 1994; Schall *et al.*, 1996).

The purpose of this study is to systematically investigate the correlation between supersaturation and crystal quality. We focused on two possibilities for the correlation between supersaturation and crystal quality: (i) the possibility that misoriented incorporation of protein molecules is increased by fast crystal growth at high supersaturation and (ii) the possibility that macroscopic defects are increased by supersaturation. AFM observations revealed the actual crystal surface morphology and the growth rate of lysozyme crystals in various supersaturated solutions. X-ray synchrotron diffraction experiments were then performed to detect the overall difference in molecular ordering. The use of synchrotron radiation was crucial in order to detect the quality difference of lysozyme crystals, which diffracted fairly well. Highly purified lysozyme was used as a model protein in order to neglect the effects of impurity incorporation. The correlation of supersaturation, surface morphology, growth rate and the crystal quality will be described in this article.

2. Methods

2.1. Sample purification

Hen egg-white (HEW) lysozyme (molecular weight 14 300 Da) was used for our research as a classic model protein. Lysozyme has been well characterized by both experimental and theoretical analyses. It is commercially available and has been the standard sample for protein crystal-growth studies. Sixfold-recrystallized lysozyme was used throughout this study (Cat. No. 100940, lot E98302, Seikagaku Kogyo Co. Ltd). The sample was purified to 99.99%(*w*/*w*) in order to exclude the possibility of impurity incorporation. We followed the purification protocol reported previously (Thomas *et al.*, 1996; Nakada *et al.*, 1999). Commercially purchased lysozyme was purified by recrystallization and cation-exchange high-pressure liquid chromatography (HPLC) column. Through this purification process, contaminants (covalent dimers and other impurities) were reduced to a concentration below 0.01%(*w*/*w*). This was determined by sodium dodecylsulfate–polyacrylamide gel electrophoresis (SDS–PAGE) using Sypro Orange dye. The impurity band was barely observed in the gel image read by FLA2000 (Fujifilm) when a 30 µg sample was loaded, while the detection limit of Sypro Orange dye was 1–0.5 ng in this detection system.

2.2. AFM observation

For AFM observations, tetragonal lysozyme seed crystals were prepared. The (110) surface of the seed crystal was used as a substrate to monitor surface morphology in various supersaturated solutions. The seed crystals were crystallized by the batch method at 293 K, in a solution of 100 mg ml^{-1} lysozyme, 25 mg ml^{-1} NaCl and 50 m*M* sodium acetate buffer pH 4.5. These seed crystals were allowed to grow for one week in order to let the crystal surface smoothen. This was necessary in order to use the seed-crystal surface as a substrate to accurately reflect the growth mode in each supersaturated solution.

The seed crystals were grown on a glass substrate and placed at the bottom of a fluid cell filled with the mother solution. The sample stage was controlled at 293 $\pm$ 0.3 K by a coolant system. Just prior to the AFM observation, the mother solution in the cell was replaced by the supersaturated solution prepared at 293 K. Various supersaturated solutions were examined (S = 1–8). Since the lysozyme solubility in 25 mg ml^{-1} NaCl and 50 m*M* sodium acetate buffer pH 4.5 at 293 K is known to be 15 mg ml^{-1} (Sazaki *et al.*, 1996), the

Table 1
Crystal data and data-collection statistics.

The growth conditions were determined from our AFM observations.

Sample	*a*	*b*	*c*	*d*	*e*	*f*	*g*	*h*	*i*	*j*	*k*	*l*	*m*	*n*
Growth condition	*A*	*A*	*B*	*B*	*B*	*B*	*B*	*B*	*C*	*C*	*C*	*C*	*C*	*C*
Supersaturation† at crystallization start	1	1	2	2	2	4	4	4	6	6	6	8	8	8
Lysozyme concentration at crystallization start (mg ml^{-1})	30	30	45	45	45	75	75	75	105	105	105	135	135	135
Supersaturation† at crystallization end	0	0	0	0	0	2.7	2.7	2.7	3.3	3.3	3.3	7.4	7.4	7.4
Lysozyme concentration at crystallization end (mg ml^{-1})	15	15	15	15	15	56	56	56	65	65	65	126	126	126
Crystallization time	3 months	3 months	2 months	2 months	2 months	2 d	2 d	2 d	24 h	24 h	24 h	12 h	12 h	12 h
Crystal dimensions (mm)	0.6	0.5	0.3	0.5	0.6	0.3	0.5	0.5	0.5	0.3	0.4	0.3	0.3	0.3
	0.3	0.3	0.2	0.4	0.3	0.3	0.25	0.3	0.4	0.25	0.3	0.3	0.3	0.3
	0.2	0.2	0.2	0.2	0.3	0.25	0.1	0.2	0.25	0.2	0.2	0.25	0.2	0.25
Illuminated crystal volume max. (mm^3)	0.003	0.003	0.002	0.004	0.003	0.003	0.0025	0.003	0.004	0.0025	0.003	0.003	0.003	0.003
Illuminated crystal volume min. (mm^3)	0.002	0.002	0.002	0.002	0.003	0.0025	0.001	0.002	0.0025	0.002	0.002	0.0025	0.002	0.0025
Oscillation angle (°)	1	1	1	1	1	1	1	1	1	1	1	1	1	1
No. of images	180	102	98	180	180	180	180	180	180	180	180	180	180	180
Unit-cell parameters (Å)														
a, *b*	78.94	79.12	79.14	79.09	79.10	79.14	79.14	79.22	79.13	79.11	79.13	79.08	79.14	79.13
c	38.21	38.10	38.12	38.12	38.12	38.01	38.00	37.97	38.00	38.04	38.03	38.03	37.97	38.00
Standard deviations of the unit-cell parameters														
a, *b*	0.054	0.012	0.007	0.002	0.001	0.006	0.004	0.006	0.006	0.006	0.007	0.004	0.029	0.009
c	0.060	0.004	0.002	0.003	0.002	0.000	0.002	0.003	0.006	0.003	0.008	0.001	0.019	0.002
Maximum resolution limit (Å)	1.39	1.4	1.42	1.41	1.42	1.45	1.48	1.47	1.42	1.6	1.38	1.55	1.46	1.41
Number of unique reflections‡	16390	16420	16427	16394	16422	16408	16285	16431	15979	16414	16395	16357	16398	16403
Overall completeness‡ (%)	99.5	99.5	99.6	99.4	99.5	99.6	99.1	99.6	97.5	99.6	99.6	99.5	99.6	99.6
Completeness (%) in the highest resolution shell§	100	99.6	100	99.6	99.6	100	99.1	100	97.1	100	99.8	100	100	100
Average $\langle I\rangle/\langle\sigma(I)\rangle$‡	8.9	9.1	8.1	8.9	8	7.3	6.4	7.7	5.1	6.5	8.6	4.7	7.7	7.9
$\langle I\rangle/\langle\sigma(I)\rangle$ in the highest resolution shell§	5.7	5.9	4.9	5.4	5.3	4.1	3.7	3.8	4.4	2.1	5.8	2.3	4.1	5.1
Overall $R_{\rm merge}$¶ (%)	4.6	4.3	4.8	4.5	4.7	5.4	6	5.3	6.4	6.6	4.5	8.1	5.2	5
$R_{\rm merge}$ in the highest resolution shell§ (%)	12.5	12.6	14.9	13.2	14	17	19.5	19.5	15.3	32.1	12.7	24.9	18.1	14.4
Overall *B* factor calculated from the Wilson plot	17.27	17.92	17.97	17.45	18.22	17.43	17.04	17.45	17.52	17.29	17.65	17.51	17.37	17.68
Multiplicity	14.0	7.90	7.60	14.0	14.0	13.9	14.1	14.0	14.2	14.0	14.0	13.3	14.0	14.0

† Supersaturation (S) was calculated as follows: $S = C - {\rm Ce}/{\rm Ce}$ (C, lysozyme concentration; Ce, lysozyme solubility at 293 K). ‡ Calculated in the range 10–1.6 Å. § Value for the highest resolution shell (1.69–1.6 Å). ¶ $R_{\rm merge} = \sum|I_i - \langle I\rangle|/\sum I_i$, where I_i is the measured intensity of an individual reflection and $\langle I\rangle$ is the mean intensity of symmetry-related equivalent reflections.

supersaturation was calculated as described previously. After replacing the solution in the cell, the AFM cantilever was immediately brought up to the crystal surface for observation.

The observation was performed by contact mode AFM (Seiko Instruments Inc.). The scanner size was 150 × 150 µm, the spring constant of the Si_3N_4 cantilever was 0.02 N m^{-1} and the scanning rate was 2–3 Hz. Different crystals were used for each experiment in order to accurately reflect the surface morphology in each supersaturated solution.

2.3. Sample preparation for X-ray data collection

Tetragonal crystals for X-ray data collection were crystallized by the conventional batch method at a temperature of 293 K. Lysozyme stock solution was mixed with NaCl solution and buffer to prepare S = 1, 2, 4, 6, 8 solutions (25 mg ml^{-1} NaCl and 50 m*M* sodium acetate buffer pH 4.5). Crystals were grown in a plastic container completely filled with crystallization solution and covered with an air-tight glass cover slip.

A metastable zone is a region in the crystallization phase diagram where the supersaturation of the solution is sufficient for growth but not for nucleation. Therefore, for S = 1 (30 mg ml^{-1} lysozyme) samples, which corresponds to the metastable zone according to our preliminary study, the microseeding method was utilized. Also, microseeding was used for S = 2 (45 mg ml^{-1} lysozyme) samples since nucleation would take a few weeks. Under these conditions, the microseeds grew slowly for two to three months until they reached a thickness of 0.2 mm. The microseeding was performed as follows. First, the seed crystals were grown with the same protocol as the seeds for AFM observation. The seeds were then crushed in 1 ml protein solution (30 mg ml^{-1} lysozyme, 25 mg ml^{-1} NaCl, 50 m*M* sodium acetate buffer) with a pipette tip and then filtered through a membrane filter (pore size 0.22 µm). The microseed solution was added to the crystallization solution in a 1%(*v*/*v*) ratio. The microseeds were then grown in the same batch-method apparatus described previously.

To summarize, the S = 1 (samples *a* and *b* in Table 1) and S = 2 crystals (samples *c*, *d* and *e* in Table 1) were grown from microseeds. The microseeds grew in the batch-method apparatus filled with S = 1 and S = 2 solution. S = 4, 6, 8 crystals (samples *f*, *g*, *h*, samples *i*, *j*, *k* and samples *l*, *m*, *n*, respectively, in Table 1) were grown by the same batch-method apparatus without microseeds. These crystals grew from spontaneous nucleation.

The lysozyme concentration in the batch container decreases owing to protein consumption by the growing crystals. Therefore, great care was taken to pick the first set of crystals that appeared in each batch; otherwise, crystals that appeared later may have started growing in a much lower supersaturation than intended. The protein concentration in the mother solution was checked before the crystals were mounted for X-ray diffraction experiment. These supersaturation data and the crystallized duration data are listed in Table 1. All crystals experienced a decrease in supersaturation during their growth.

In general, crystals grown from low supersaturation tended to be markedly longer in shape than those grown at high supersaturation. The crystal morphology changed according to the supersaturation; the {101} surface developed faster than the {110} surface at lower supersaturation, yielding rod-shaped crystals surrounded by {110} faces (the long axis is the *c* axis), consistent with previous reports (Monaco & Rosenberger, 1993; Judge *et al.*, 1999). All crystals were well faceted and no obvious defects were noted by microscopic observation.

Just after the crystals grew to their maximum thickness of 0.2 mm, they were transferred to the synchrotron facility and were subjected to X-ray diffraction study.

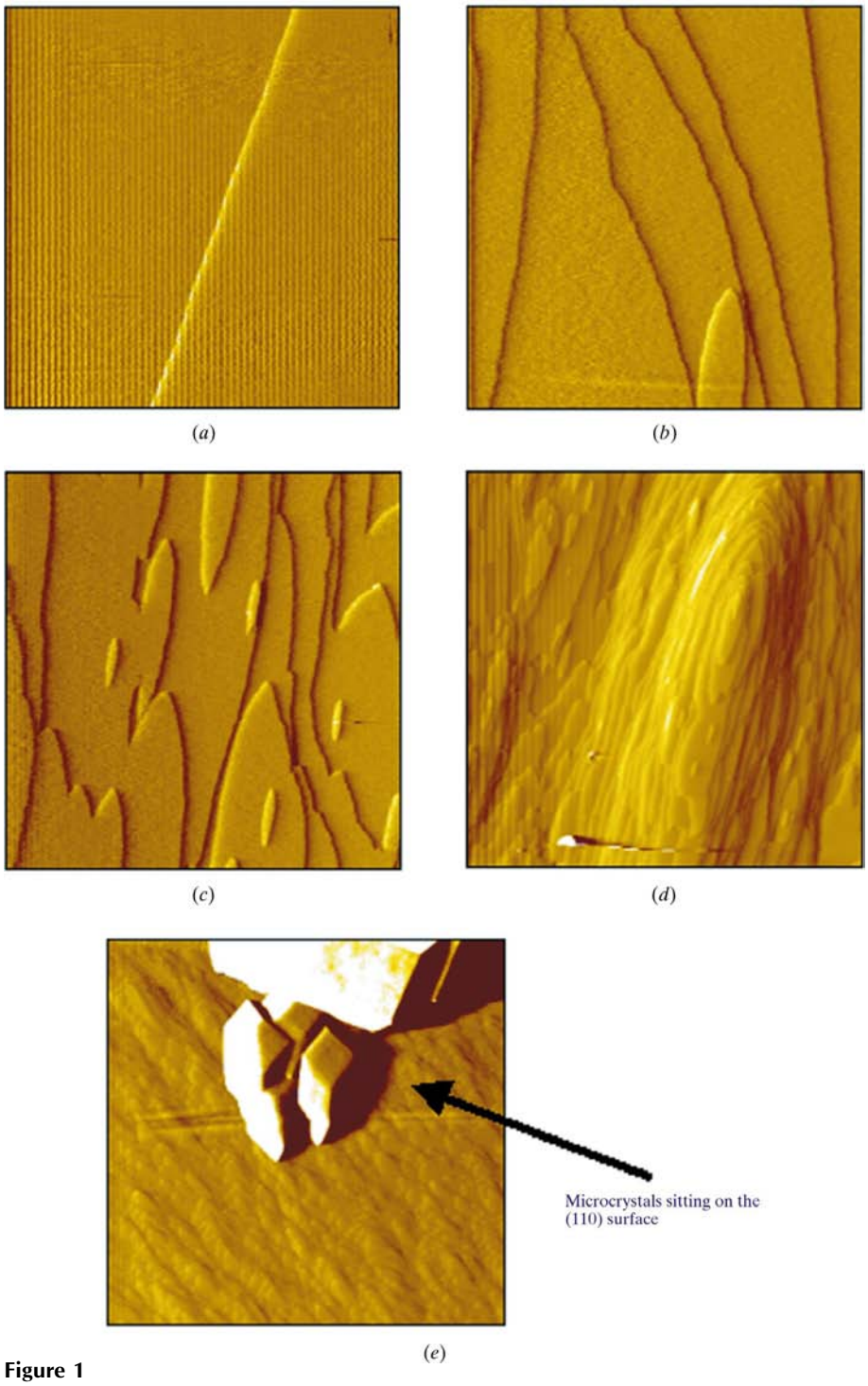

Figure 1
AFM images of the (110) surface of a tetragonal lysozyme crystal in supersaturated protein solution. The images represent 15 μm square. (*a*) Surface image in the $S = 1$ solution. No 2D nucleation is observed. The steps on the seed crystals are proceeding forward. (*b*) Surface image in the $S = 2$ solution. Note some 2D islands forming and spreading. No screw dislocation was observed. (*c*) Surface image in the $S = 3$ solution. The numbers of 2D islands increases as a function of supersaturation. (*d*) Surface image in the $S = 8$ solution. Note the rapid 2D nucleation causing steep hills and some regions left behind that look like valleys. (*e*) Surface image showing microcrystals on the seed-crystal surface. Microcrystals were embedded into the growing crystal as growth proceeded.

2.4. X-ray data collection and processing

Crystals were mounted just prior to X-ray diffraction data collection. Crystals were picked from the top lid of the batch apparatus where they had adhered. In every case, one crystal was mounted in a 2.0 mm thin-walled glass capillary with the long axis (*c* axis) of the crystal along the capillary axis. Therefore, the X-ray beam was perpendicular to the longer axis. Thus, the thickness of the crystal was regarded to be more important than its length. Since a highly directive X-ray beam was utilized, the illuminated crystal volume could be calculated as 0.1 mm × 0.1 mm (collimator size) × (crystal thickness) mm. Therefore, although the crystals grown at lower supersaturation were morphologically longer, the actual illuminated volume was effectively the same as that of other crystals. Dimensions of the lysozyme crystals used for data collection and

the actual illuminated crystal volume are summarized in Table 1.

All data were collected at room temperature at BL-6A of the Photon Factory (PF), Tsukuba, Japan. Nearly complete diffraction data sets were collected using an ADSC Quantum 4R CCD detector by the oscillation method with a wavelength of 1.0 Å. 14 samples were analyzed in total, with special attention paid to keeping the experimental procedure and data-collection protocol strictly the same. The crystal-to-detector distance was 100 mm in order to obtain adequate reflection separation. The oscillation angle was 1° and the exposure time of 10 s per image was constant for all samples. Most crystals yielded 180 images with a high multiplicity of around 14, but two samples yielded only 102 and 98 processible images owing to experimental restrictions. To avoid sample damage and to save time, dezingering (*i.e.* taking two identical exposures and removing differences to compensate for the detection of random environmental radiation) was not used.

The X-ray diffraction data were processed in four steps. The images were autoindexed and integrated using the programs *DPS*/*MOSFLM*/*CCP*4 (Rossman & van Beek, 1999) and then merged and scaled together with *SCALA*/*CCP*4 (Collaborative Computational Project, Number 4, 1994) using batch scales and smoothing of *B* factors. This provided standard crystallographic statistics on crystal quality such as the maximum resolution limit, $\langle I\rangle/\langle\sigma I\rangle$, overall *B* factor, $R_{\rm merge}$ and mosaicity. The space group was $P4_32_12$, with unit-cell parameters $a = b = 79.1$ (1), $c = 38.0$ (1) Å.

3. Results

3.1. Crystal surface morphology observation by AFM

The AFM observation was conducted to examine the surface morphology and growth rate at various supersaturations. Using a small protein molecule such as lysozyme, it is quite difficult to detect point defects or molecular misorientations. However, AFM is suitable for visualizing the growth mode, which is likely to change according to the supersaturation and is apt to affect the crystal quality (Ng *et al.*, 1997). We also attempted to detect planar defects, stacking faults and dislocations that may also affect the crystal quality (Malkin *et al.*, 1996).

Fig. 1(*a*) shows a typical AFM image of a (110) surface of a tetragonal seed crystal in the $S = 1$ (30 mg ml^{-1} lysozyme) solution. No two-dimensional (2D) nucleation or spiral growth was observed in a 1 h observation period. The steps just proceeded forward slowly in the $S = 1$ solution. The fact that 2D islands were not observed indicates that the $S = 1$ solution does not provide enough driving force to create 2D islands. This means that screw dislocation must occur in order to supply new steps on the crystal surface in the $S = 1$ solution according to the classical theory. To maintain crystal growth, there must be screw dislocations somewhere on the surface, although spiral growth was not found during our observation.

Fig. 1(*b*) shows the crystal surface in the $S = 2$ (45 mg ml^{-1} lysozyme) solution. 2D islands were occasionally observed to form on the terraces. The islands grew and merged with proceeding steps or neighbouring islands. In solutions of $S = 3$ (60 mg ml^{-1} lysozyme) and $S = 4$ (75 mg ml^{-1} lysozyme), 2D islands appeared more frequently and the growth rate increased as expected (Fig. 1*c*).

A drastic change in surface morphology was observed in solutions $S = 5$ (90 mg ml^{-1} lysozyme) to $S = 8$ (135 mg ml^{-1} lysozyme). As seen in Fig. 1(*d*), 2D islands kept forming and spreading at a very high speed. The height of each 2D island was around 5 nm, equivalent to two lysozyme molecules in height. This was the same step height as in Figs. 1(*a*), 1(*b*) and 1(*c*). This means the 2D islands observed in $S = 5$–8 are not anything unusual, but are ordinary 2D islands. The growth speed was undetectable because the 2D islands kept piling on top of other islands. As a result, when we finished one scan and went to the next scan, the island that we had been looking at was already buried in the next growth layer. The islands kept forming on top of other islands and resulted in steep hills. In contrast, there were some regions left behind that looked like valleys. This behaviour could be interpreted as follows. The protein concentration is always lower at the crystal surface than the bulk solution since the crystal surface incorporates protein molecules. Because the 2D nucleation occurs very rapidly in a highly supersaturated solution, when one 2D island forms on top of another 2D island, the upper 2D island will be closer to the bulk solution (where the protein concentration is higher). This makes it easier for the next 2D island to form on top of the second 2D island than on the lower crystal surface (where the protein concentration is lower). Once this cycle starts, it is difficult to fill in the valley part left behind until the bulk concentration decreases.

The surface morphology described here was reproducible over multiple and iterative experiments involving different crystals. Therefore, from these AFM observations, we classified the growth conditions into three categories: *A*, in which 2D island growth did not take place ($S = 1$; low supersaturation), *B*, 2D growth ($S = 2$–4; moderate supersaturation) and *C*, rapid 2D growth ($S = 5$–8; high supersaturation). Of course, the growth speed (molecule intake speed) increased in the order *A*, *B*, *C*.

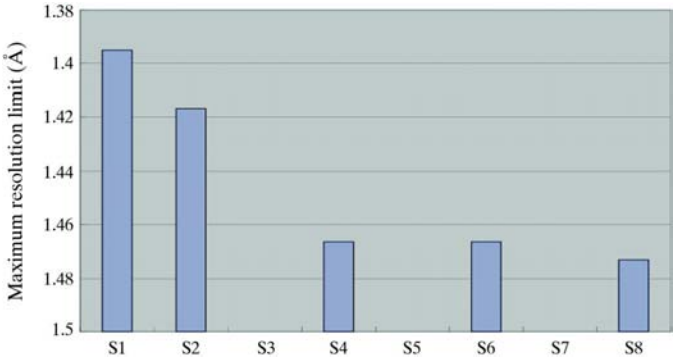

Figure 2
Average maximum resolution limit of crystals from each supersaturation condition. Here it is clearly shown that there is a linear correlation between the supersaturation and the resolution.

Another significant observation was that microcrystals (and macroclusters) frequently settled on the crystal surface in higher supersaturated conditions as we continued our observation (Fig. 1*e*). This is expected to happen because nucleation frequency increases exponentially as a function of supersaturation. This microcrystal in Fig. 1(*e*) was embedded into the larger crystal as the larger crystal kept growing (consistent with previous reports; for example, Kuznetsov *et al.*, 1996). However, no other major defects, except for microcrystal incorporation, were observed even at higher supersaturation. Adhesion growth that causes kinetic roughening was not observed either.

In summary, three major differences were found in the crystal-growth behaviour in conditions *A*, *B* and *C*: 2D nucleation frequency, growth speed and microcrystal sedimentation frequency. In the next step, we attempted to investigate the inner order of the crystals by X-ray diffraction studies and to verify the correlation between the phenomena observed by AFM and X-ray diffraction.

Since the effect of microcrystals on the degeneration of crystal quality is obvious, we decided to focus on the effect of 2D nucleation and the growth speed. Therefore, we tried to choose crystals that did not contain microcrystals. To minimize the possibility of selecting crystals containing microcrystals, we chose crystals that adhered to the top lid of the crystallization container. This way, the crystals that we selected would at least not contain the large microcrystals that would normally be deposited.

If 2D nucleation and growth speed affect the crystal quality, we predict that 2D island growth may affect the crystal perfection because when the islands meet and merge, the molecules at the island interface may fail to align in the correct lattice position. Crystals grown under condition *C* may be especially affected by macrodefects arising from 2D island hills. The high growth rate may also affect the crystal quality by molecular misorientation at the kink site. These possibilities cannot be proved directly currently because of the difficulty in detecting the misorientations of each of the protein molecules. Therefore, X-ray diffraction studies were applied. Though indirect, the diffraction properties will show the total level of molecular ordering in the crystal.

3.2. X-ray diffraction

3.2.1. Diffraction properties. The maximum resolution limit was defined as the resolution when $\langle I\rangle/\langle\sigma(I)\rangle$ fell below 2. Of the 14 samples, the worst crystal diffracted to a maximum resolution limit of 1.6 Å. Therefore, in order to compare intensity data with high reliability, only reflections to 1.6 Å were used for all analysis. The data were typically obtained with an overall completeness of 97.5% or more and an $R_{\rm merge}$ below 11%. In the highest resolution shell (1.69–1.6 Å), completeness exceeded 97.1% and $R_{\rm merge}$ was less than 32%. Data multiplicity was 13.3–14.2 overall (except for the two samples described previously), which enabled good statistics. There were about 16 400 unique reflections to 1.6 Å.

There are some generally accepted criteria for assessing the crystal quality, such as the maximum resolution limit, $\langle I\rangle/\langle\sigma(I)\rangle$, $R_{\rm merge}$, overall *B* factor and mosaicity.

The maximum resolution limit directly shows the diffracting power of the crystals. If the protein molecules are well packed and aligned, they are expected to diffract well. The average resolution of the crystals from each supersaturated solution is shown in Fig. 2. A clear tendency is noted in which crystals from lower supersaturated solutions diffracted better. $\langle I\rangle/\langle\sigma(I)\rangle$ is the signal-to-noise (S/N) ratio of the diffracted intensity, where I is the reflection intensity and $\sigma(I)$ is the standard deviation obtained by merging symmetry-related reflections. This criterion also reflects the diffracting power of the crystals. Fig. 3 shows the $\langle I\rangle/\langle\sigma(I)\rangle$ value for the crystals from each supersaturated solution. A reduction of the intensity S/N ratio is noted along the x axis (supersaturation). $R_{\rm merge}$ is an overall measure of the errors within a data set. It compares the differences between symmetry-related reflections that should ideally be identical in intensity. Fig. 4 shows the $R_{\rm merge}$ value, where a linear increase in the errors is evident.

The overall *B* factor was calculated from the Wilson plot in the range 3.0–1.6 Å. The *B*-factor difference may reflect

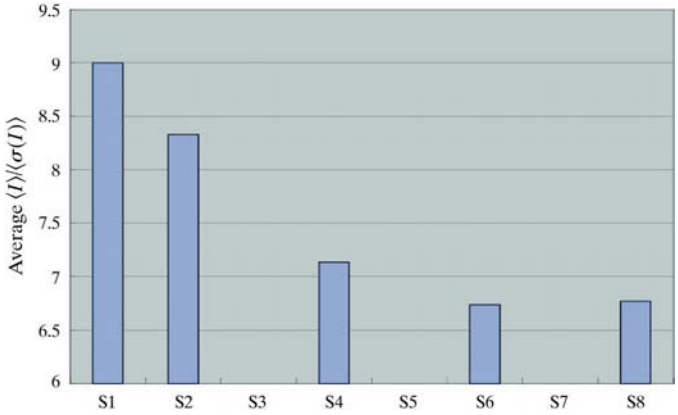

Figure 3
Average $\langle I\rangle/\langle\sigma(I)\rangle$ of crystals from each supersaturation condition. Here it is clearly shown that there is a linear correlation between the supersaturation and $\langle I\rangle/\langle\sigma(I)\rangle$.

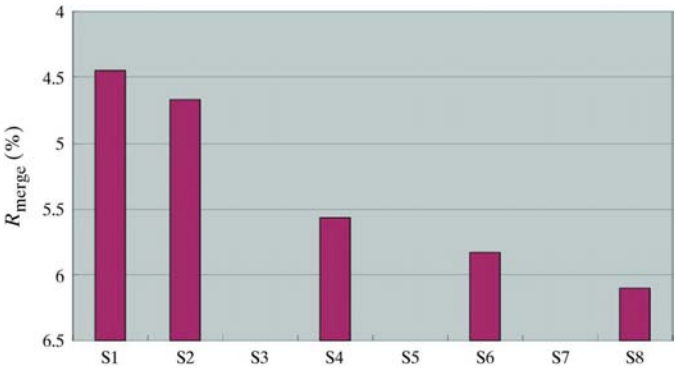

Figure 4
Average $R_{\rm merge}$ of crystals from each supersaturation condition. Here it is clearly shown that there is a linear correlation between the supersaturation and $R_{\rm merge}$.

thermal vibration, conformational disorder or static lattice disorders of protein molecules (misorientation). The internal order is expected to be estimated from the *B* factor. From the results obtained so far (Figs. 2, 3 and 4), it seems that crystals grown at higher supersaturations were less ordered. However, no direct correlation was found between the supersaturation and the *B* factor. It turned out that the *B* factor did not directly reflect the degree of misoriented molecules caused by high supersaturation. Unknown or complicated causes may have affected the *B*-factor value.

The mosaicity was also estimated from the *DPS*/*MOSFLM*/*CCP*4 software, but the differences from the original mosaic spread of the lysozyme crystal were too small to quantitatively evaluate the correlation with supersaturation.

The values of these factors for each crystal are summarized in Table 1. It was apparent from these data that crystals grown from low supersaturated solutions yielded better diffraction properties than crystals grown from highly supersaturated solutions (except for the *B* factor). We performed statistical analysis to quantitatively evaluate this correlation.

3.2.2. Quantitative evaluation of diffraction results. In order to quantitatively evaluate the correlation of supersaturation and these criteria of crystal quality, we performed tests by stepwise regression analysis for all 14 samples using the multiple regression and general linear model in the statistics program. The contributing predictor was selected in the model in order to add strong predictors and/or in order to statistically predominate by eliminating weak predictors. The factor [supersaturation] was dependent on [crystallized time] (the term in brackets indicate the selected predictor used for analysis in the statistics). Therefore, supersaturation definitely correlates with the crystal-growth rate. It involves balancing the predictive power (the multiple correlation coefficient, *R*) against the statistical significance (the probability value, *P*) estimated from the analysis of the variance (ANOVA) of the data sets if the one selected factor was used. The model reproduced the observed variability very well – the regression coefficient was close to 1.0 (the correlation coefficient $R = 0.853$) and is statistically very significant – the *F* ratio had very low probability ($P = 0.000$). Therefore, supersaturation was allowed to be a factor contributing to the enhanced quality of crystal as [crystallized time].

[Supersaturation] also depends on each selected single factor such as $[\langle I\rangle/\langle\sigma(I)\rangle]$ with the correlation coefficient $R = 0.593$ ($P = 0.026$), [maximum resolution limit] with $R = 0.525$ ($P = 0.054$) and $[R_{\rm merge}]$ with $R = 0.593$ ($P = 0.026$). If the crystal is grown at lower supersaturation, it is expected to diffract to a higher resolution limit with better intensity data sets and with less error. The intensities of the crystals grown in lower supersaturated solution improved significantly, regardless of the term [illuminated crystal volume].

As mentioned before, although the overall *B* factor is an isotropic temperature factor estimated from the Wilson plot, it did not correlate with [supersaturation]. Rather, [*B* factor] depends on the two terms [illuminated crystal volume] and [the unit cell] ($R = 0.901$, $P = 0.001$). The favourable [variation of the unit cell] effect overbalanced the adverse effect of [illuminated crystal volume]. When the unit cell size is larger, the illuminated crystal volume is actually larger and the *B* factor is roughly estimated to be lower from the Wilson plot.

It is worth noting that a statistically significant correlation between supersaturation and unit-cell parameters was found ($R = 0.879$, $P = 0.000$). The growth-rate dependency of the {110} and {101} faces on supersaturation differ, which causes morphology differences at different supersaturations (as stated before). In particular, the supersaturation is proportional to the variation of the unit-cell parameter in the crystallographic *c* axial direction (Monaco & Rosenberger, 1993; Judge *et al.*, 1999). Fig. 5 shows the change of the unit-cell parameter in the *c* direction *versus* supersaturation. Though the variance of the unit-cell parameter is buried within the standard deviation of measurement error, this may imply that higher supersaturation yielded a shorter *c* axis. This will be investigated further, including the cause of this correlation.

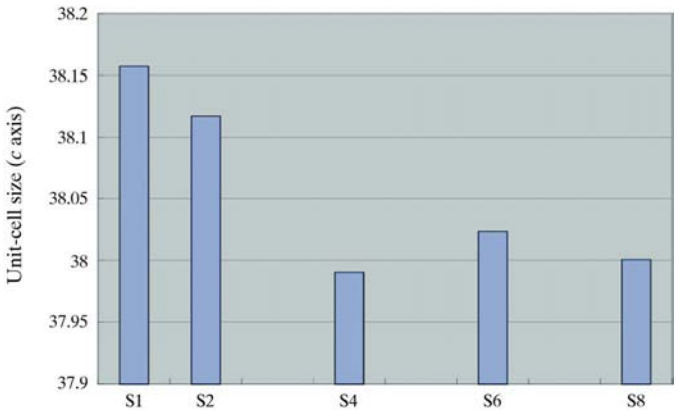

Figure 5
Average *c* axis unit-cell parameter of crystals from each supersaturation condition. Here it is clearly shown that there is a linear correlation between the supersaturation and the *c*-axis length.

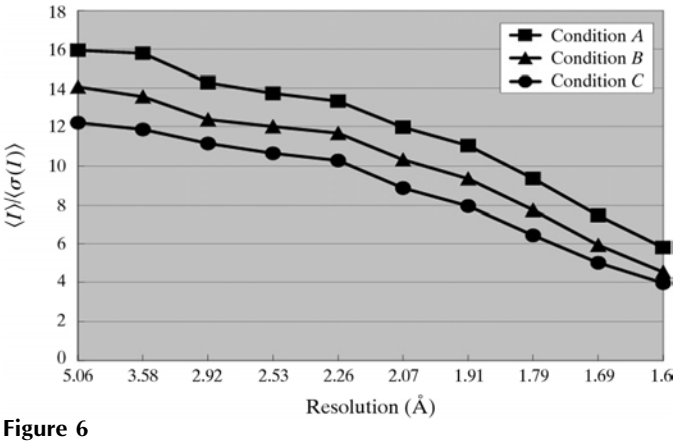

Figure 6
Plot showing the mean $\langle I\rangle/\langle\sigma(I)\rangle$ (*y* axis) *versus* resolution, $1/d^2 = 4\sin^2\theta/\lambda^2$ (Å^{-2}) (*x* axis). Standard deviations σ were obtained by merging symmetry-equivalent reflections. The diffraction intensity data of crystals grown in low (condition *A*, squares), moderate (condition *B*, triangles), high (condition *C*, circles) supersaturation are plotted. Note the significant difference in diffraction data between conditions *A*, *B* and *C*.

3.2.3. Crystal quality differences between crystals grown under conditions *A*, *B* and *C*. The quality differences of crystals grown under conditions *A*, *B* and *C* according to the AFM observations were evaluated. X-ray diffraction study provided reliable statistics for assessing the crystal quality. From our statistics, the $\langle I\rangle/\langle\sigma(I)\rangle$ value was found to be one of the appropriate factors for evaluating the crystal quality.

Fig. 6 shows the mean $\langle I\rangle/\langle\sigma(I)\rangle$ as a function of resolution of crystals grown in conditions *A*, *B* and *C*. $\langle I\rangle/\langle\sigma(I)\rangle$ was relatively higher in the order *A*, *B*, *C* across the resolution. The $\langle I\rangle/\langle\sigma(I)\rangle$ value of condition *A* is constantly 1.3 to 1.5 times higher than that of condition *C*. This implies that the S/N ratio of the reflections that make up the diffraction pattern increases uniformly at lower supersaturation. The molecular orientation at the lattice point must have been better.

The correlation between the maximum resolution limit and supersaturation was also considered as statistically significant. The average resolution of crystals grown in condition *A* was 1.39 Å, while the average resolution of crystals grown in condition *C* was 1.47 Å. This is quite a difference considering that all the lysozyme crystals diffracted very well.

The $R_{\rm merge}$ value of the diffraction data also exhibits internal consistency. The average $R_{\rm merge}$ value varied from 4.5% (crystals from condition *A*) to 6.0% (crystals from condition *C*).

4. Discussion

The same experimental setup allowed reliable collection of 14 sets of oscillation data from crystals grown in various supersaturated conditions. Diffraction properties, such as the maximum resolution limit, the conventional crystallographic parameters $\langle I\rangle/\langle\sigma(I)\rangle$ and $R_{\rm merge}$, were obtained and analyzed. These properties were used to compare the quality of crystals grown in different supersaturation conditions.

This systematic study has proved there is a statistically significant correlation between supersaturation and $\langle I\rangle/\langle\sigma(I)\rangle$. Both the increase of peak intensities and the reduction of background of the crystals grown in lower supersaturated conditions improved significantly compared with those of crystals grown in both moderate and high supersaturated conditions. In contrast, no correlation was found between the illuminated crystal volume and $\langle I\rangle/\langle\sigma(I)\rangle$. Therefore, the results are not a result of the illuminated crystal volume, but are solely dependent on supersaturation. This implies that lower supersaturation levels produce larger homogeneous diffracting regions, whereas the molecules were well ordered. The statistical correlation between supersaturation and the maximum resolution limit and $R_{\rm merge}$ also supports our conclusion.

Showing the mosaic spread of those crystals grown in different conditions is very persuasive. These statistics would be useful, along with the measurement of rocking curve, in future comparative studies.

The seeding technique is not a popular crystallization method in protein crystal growth. However, our data show that crystals grown from microseeds in low supersaturated conditions diffracted significantly better than the crystals grown from spontaneous nucleation. The seeds were made at a high supersaturation level (S = 5.7) and then crushed to produce microseeds. Next, the microseeds were added to the S = 1 and 2 solutions. Our results shows that protein crystals do not necessarily retain the crystal habits or defects from their seed crystal. The growth condition is the important factor. The use of seed crystals at low supersaturation should be promoted.

The crystals subjected to X-ray diffraction studies grew in solutions whose initial supersaturation levels were defined. As growth proceeded, the supersaturation of the solution decreased as shown in Table 1. If the correlation between the supersaturation and unit-cell size was real, it is probable that the unit-cell size of the crystal gradually changed as growth proceeded. Split-spot profiles or discernible shoulders of the Bragg diffraction reflection may occur in these cases. This appears to cause lattice strain and to produce larger mosaicity in the crystal. This long-range lattice change may also be included in our X-ray diffraction results. The lattice change discussed above may have affected the result, especially in the S = 2, 4, 6 samples, since a large supersaturation change took place during its growth. In contrast, S = 8 samples experienced smaller supersaturation changes during their short growth period and the quality of two of the samples (samples *m* and *n* in Table 1) is almost as good as the quality of S = 4 or 6 crystals. This may mean that supersaturation change during growth significantly affects the crystal quality. To confirm the possibility of lattice-parameter change according to the supersaturation, we must grow crystals at constant supersaturation. Schall's method with a temperature-control system will be useful (Schall *et al.*, 1996).

Considering the results obtained so far, the AFM results match the X-ray diffraction results very well and there seems to be no contradiction between them. They are also consistent with a previous study that reported the same tendency in resolution (Ng *et al.*, 1997). Going back to our question about why high supersaturation would affect the crystal quality, it turns out that molecular misorientation is the cause.

In the AFM observations, no obvious crystal defect was observed except for the sedimentation of microcrystals and macroclusters in higher supersaturated conditions. Since crystals were selected from the top lid of the crystal-growth container, the possibility of microcrystal incorporation was minimized. Therefore, the only differences in crystals grown under conditions *A*, *B* and *C* were the 2D nucleation frequency and the growth rate. High hills and deep valleys were created in condition *C* samples, but the fact that S = 1, S = 2 and S = 4 samples showed a significant difference in quality indicates that this hill formation itself was not the major reason for the quality degeneration at higher supersaturation levels. Also, the fact that S = 1 samples were much better in quality than S = 8 samples (although the supersaturation change was about the same) demonstrated that the supersaturation change was also not the major reason. We speculate that the molecular misorientations caused by the 2D islands merging together and by the high growth rate (fast

molecular intake) at the kink site were the main cause. Though there is no way to visualize these molecular misorientations directly, X-ray diffraction could indeed detect the difference in inner order. It is convincing that the inner order of the crystals grown slowly in low supersaturated conditions with fewer 2D islands was significantly better and improved the diffraction quality.

5. Conclusions

Supersaturation produces enormous effects on the crystal properties of proteins. X-ray synchrotron diffraction clearly demonstrated that there was a strong correlation between supersaturation and the diffracting power of the crystal. The crystals grown in lower supersaturated conditions diffracted to a higher resolution limit with better intensity data sets and with fewer errors. Together with the AFM observations, our results strongly suggest that molecular misorientations affect the crystal quality. A high throughput can be achieved in today's structural biology by taking supersaturation into account. If many crystals are obtained in a very short time, the crystals may be growing in an extreme supersaturated condition. It is worthwhile to try to simply reduce the protein concentration or precipitant concentration or change the temperature to reduce the supersaturation in order to obtain better quality crystals.

The authors thank Mr Y. Iimura for sample purification. We thank the Photon Factory for the beamtime allocated for this study. This work was performed with the approval of the Photon Factory Advisory Committee, Japan (proposal No. 2000 G316).

References

Boggon, T. J., Helliwell, J. R., Judge, R. A., Olczak, A., Siddons, D. P., Snell, E. H. & Stojanoff, V. (2000). *Acta Cryst.* D**56**, 868–880.
Chernov, A. A. (1984). In *Modern Crystallography*, Vol. III: *Crystal Growth.* Berlin: Springer-Verlag.
Collaborative Computational Project, Number 4 (1994). *Acta Cryst.* D**50**, 760–730.
Judge, R. A., Jacobs, R. S., Frazier, T., Snell, E. H. & Pusey, M. L. (1999). *Biophys. J.* **77**, 1585–1592.
Kuznetsov, Y. G., Malkin, A. J., Glantz, W. & McPherson, A. (1996). *J. Cryst. Growth*, **168**, 63–73.
Malkin, A. J., Kuznetsov, Yu. G. & McPherson, A. (1996). *J. Struct. Biol.* **117**, 124–137.
Monaco, L. A. & Rosenberger, F. (1993). *J. Cryst. Growth*, **129**, 465–484.
Nakada, T., Sazaki, G., Miyashita, S., Durbin, D. S & Komatsu, H. (1999). *J. Cryst. Growth*, **196**, 503–510.
Ng, J. D., Kuznetsov, Y. G., Malkin, A. J., Keith, G., Giegé, R. & McPherson, A. (1997). *Nucleic Acids Res.* **25**, 2582–2588.
Rossmann, M. G. & van Beek, C. G. (1999). *Acta Cryst.* D**55**, 1631–1640.
Saridakis, E. E. G., Stewart, P. D. S., Lloyd, L. F. & Blow, D. M. (1994). *Acta Cryst.* D**50**, 293–297.
Sazaki, G., Kurihara, K., Nakada, T., Miyashita, S. & Komatsu, H. (1996). *J. Cryst. Growth*, **169**, 355–360.
Schall, C. A., Riley, J. S., Li, E., Arnold, E. & Wiencek, J. M. (1996). *J. Cryst. Growth*, **165**, 299–307.
Stura, E. A. & Wilson, I. A. (1992). *Crystallization of Nucleic Acids and Proteins*, edited by A. Ducruix & R. Giegé, pp. 99–126. New York: Oxford University Press.
Thomas, B. R., Vekilov, P. G. & Rosenberger, F. (1996). *Acta Cryst.* D**52**, 776–784.